Temporal Evolution of Self-Modulated Laser Wakefields Measured by Coherent Thomson Scattering

A. Ting,[1] K. Krushelnick,[2] C. I. Moore,[1] H. R. Burris,[1] E. Esarey,[1] J. Krall,[1] and P. Sprangle[1]
[1]*Plasma Physics Division, Naval Research Laboratory, Washington D.C. 20375*
[2]*Laboratory of Plasma Studies, Cornell University, Ithaca, New York 14853*
(Received 20 June 1996)

Coherent Thomson scattering of a picosecond probe laser was used to measure the time evolution of plasma wakefields produced by a high intensity laser pulse (7×10^{18} W/cm^2) in an underdense plasma ($n_e \approx 10^{19}$ cm^{-3}) in the self-modulated laser wakefield accelerator configuration. Large amplitude plasma wakefields which lasted less than 5 ps were observed to decay into ion acoustic waves. The time scales associated with these measurements were consistent with the effects of the modulational instability and the enhancement of scattered signal from plasma channel formation. [S0031-9007(96)02018-2]

PACS numbers: 52.40.Nk, 41.75.Lx, 52.35.Mw

Significant progress has been made in recent years [1] in the use of laser-produced plasma as a medium for accelerating electrons to high energies. In the laser wakefield accelerator (LWFA) [2], a high intensity laser pulse is focused into an underdense plasma with a pulse duration, τ_L, similar to the electron plasma period (i.e., $\tau_L \sim 2\pi/\omega_{\rm pe}$, where $\omega_{\rm pe}$ is the electron plasma frequency). Large amplitude plasma waves (wakefields) are generated with strong longitudinal electric fields and relativistic phase velocities which are capable of accelerating injected electrons. For laser powers, P, approaching or exceeding the relativistic self-focusing threshold [i.e., $P_c = 17(\omega_0/\omega_{\rm pe})^2$ GW, where ω_0 is the laser frequency], it is not necessary to match the pulse duration to the plasma period. At laser powers for which $P \geq P_c$ and $\tau_L > 2\pi/\omega_{\rm pe}$, the laser envelope undergoes an instability and becomes "self-modulated" at the plasma frequency [3]. This effect resonantly enhances the creation of wakefields and allows the use of higher electron densities and generates stronger accelerating fields [4]. Recent experiments in this self-modulated laser wakefield accelerator (SM-LWFA) regime have measured the production of high energy electrons, where the source of accelerated particles was either background electrons from the target plasma [5] or electrons injected into the interaction region from an adjacent laser-produced plasma [6]. Direct observations of wakefields in the conventional LWFA configuration were recently reported using interferometric techniques, in which the spatial and temporal wave forms of the wakefield behind the pump laser pulse were measured [7].

This Letter will discuss the first experiments to use coherent Thomson scattering (CTS) of a picosecond probe laser pulse to measure the temporal behavior of self-modulated wakefields in the SM-LWFA. We confirmed the generation of wakefields with phase velocities close to the speed of light. We observed the turbulent decay of the wakefields and the transfer of energy to ion acoustic waves, possibly through a parametric process such as the modulational instability. The measured decay time of these waves is consistent with growth rates of the modulational instability for our experimental conditions. The formation of a plasma density channel behind the pump laser pulse, which can guide the probe laser pulse, could also enhance the Thomson scattered signal.

The tabletop terawatt laser at the Naval Research Laboratory is a Ti:sapphire/Nd:glass system ($\lambda = 1.054$ μm) which uses chirped pulse amplification [8] to achieve the high powers necessary for experiments in the self-modulated regime. In these experiments, the pump laser pulse had a typical duration of 400 fs and an energy of 800 mJ ($P = 2$ TW). The contrast (i.e., the ratio of the prepulse intensity to that at the peak of the laser pulse) was measured to be 10^{-6}. When the beam was focused at 1 TW by an off-axis parabolic mirror ($f/3$), the measured focal spot diameter in vacuum was 8.5 μm. This implies a peak focused intensity in our experiments of 7×10^{18} W/cm^2. For a plasma density of $n_0 \sim 10^{19}$ cm^{-3}, the critical power is $P_c \approx 1.8$ TW, and the plasma wavelength is $\lambda_{\rm pe} = 2\pi c/\omega_{\rm pe} \sim 10$ μm. Hence, $P \geq P_c$ and $c\tau_L \sim 12\lambda_{\rm pe}$, which are necessary for operation in the SM-LWFA regime.

In CTS, waves in a plasma will enhance Thomson scattered light at particular wavelengths and directions due to interference effects. Coherently scattered light has a wave vector $\mathbf{k}_{\rm sc}$ and a frequency $\omega_{\rm sc}$ that satisfy the Bragg scattering conditions of frequency and wave number matching. For electron plasma waves with $\omega_{\rm pe}$ and $\mathbf{k}_{\rm pe}$, the conditions require $\omega_{\rm sc} = \omega_1 \pm \omega_{\rm pe}$ and $\mathbf{k}_{\rm sc} = \mathbf{k}_1 \pm \mathbf{k}_{\rm pe}$, where ω_1 is the frequency and $\mathbf{k}_1$ is the wave vector of the probe laser. Plasma waves capable of accelerating electrons to high energy (as produced by a LWFA) propagate collinearly with the laser pulse and have relativistic phase velocities, $v_\phi \sim c$. CTS has also been used to measure similar relativistic ($v_\phi \sim c$) plasma waves in the laser beat-wave accelerator [9,10]. For correct matching of $\mathbf{k}$ vectors, both the probe and the Thomson scattered light must propagate in the same direction as the relativistic plasma wave (i.e., along the

pump axis of propagation). For coherent scattering to be observable, the condition $(k\lambda_D) < 1$ must be satisfied, where λ_D is the plasma Debye length and k is the wave number of the plasma waves to be measured [11]—otherwise the waves undergo severe Landau damping. In these experiments, we estimate $\lambda_D \sim 0.01$ μm and $k \sim \omega_{\rm pe}/c \sim 0.6$ $\mu{\rm m}^{-1}$.

The setup for our experiments is shown in Fig. 1. Approximately 10% of the main beam was split off by a pellicle for use as a probe pulse and was subsequently frequency doubled (to 527 nm) by a 1 cm thick KD*P crystal. For 800 mJ pump pulses the probe pulse energy was typically 10 mJ. The maximum broadening of the probe pulse length from passage through the doubling crystal will result in a pulse duration, $\tau_{L,p} < 1$ ps. This provides the intrinsic temporal resolution for our experiment. Since $c\tau_{L,p} \gg \lambda_{\rm pe}$ in these experiments, the probe pulse efficiently sampled the plasma waves it measured. This is in contrast to optical interferometric techniques [7] which require much shorter probe pulses such that $c\tau_{L,p} < \lambda_{\rm pe}$.

The probe pulse traverses a delay line and then is recombined with the main beam before being focused into the plasma created by the pump pulse. This delay line can be adjusted to vary the timing between the two pulses. The paths of the two beams were overlapped by alignment to a series of apertures prior to the focusing optics ($f/3$ off-axis parabolic mirror) as well as by observation of scattered light in the focal region. The target was a gas jet of either helium or hydrogen, and we measured the electron density by recording the wavelength shift of stimulated Raman backscattered light from interactions at lower intensities (10^{16} W/cm^2). The electron density used in these experiments was in the range of $0.5-1.2 \times 10^{19}$ cm^{-3} with ~25% of accuracy. The laser breakdown is monitored with a CCD camera at 90° to the propagation axis of the pump laser.

Coarse temporal synchronization of pump and probe pulses was achieved using a streak camera with better than 4 ps resolution. Fine temporal synchronization was attained by measuring the probe frequency after passage through the interaction region. If the probe pulse travels ahead of the pump, it ionizes the gas and generates a blue shift in the spectrum [12]. Otherwise, the frequency is unshifted. This effect is easily observed and provides a measurement of the temporal overlap to within 1 ps.

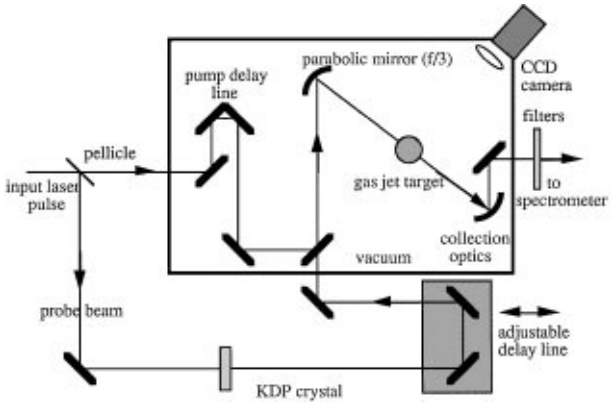

FIG. 1. Schematic of Thomson scattering experimental setup.

These experiments used two different CTS configurations. The first configuration had the pump, probe, and scattered light propagating collinearly, and unscattered light from the pump beam was attenuated by an infrared absorption filter after the interaction region. The majority of the 527 nm probe light was not scattered and was blocked before the slit of the spectrometer (0.25 m Czerny-Turner) by a notch filter in the beam path. However, the Thomson scattered electron plasma satellites of the probe light, which are shifted by $\omega_{\rm pe}$ ($\Delta\lambda_{\rm Stokes} \approx 23$ nm, $\Delta\lambda_{\text{anti-Stokes}} \approx 21$ nm for a plasma density of 7×10^{18} W/cm^{-3} as in Fig. 2), are positioned beyond the edges of the absorption band of the notch filter and hence will be detected by the spectrometer. The principal result in this configuration was the observation of these plasma satellites for about 5 ps after passage of the pump laser (see Fig. 2, which shows a FWHM of ~2 ps). As shown in the inset in Fig. 2, the anti-Stokes line was typically more intense than the Stokes line, indicating that electron plasma waves in the wakefield preferentially propagate in the forward direction [13]. These measurements confirmed the generation of wakefields with $v_\phi \sim c$ [14].

The ratio of the total scattered signal intensity to the probe intensity is given by [15], $I_s/I_1 \approx 2.5(\delta n L_z/n_{\rm cr}\lambda_1)^2$, where $n_{\rm cr}$ is the critical density for the probe wavelength (4×10^{21} cm^{-3}), λ_1 is the probe wavelength, L_z is the probe-plasma interaction length (the confocal parameter of the probe laser, ~200 μm), and δn is the density perturbation of the wave. We estimate the ratio (I_s/I_1) to be $10^{-3\pm1}$ for scattering into the electron plasma satellites. This implies that the amplitude of plasma waves encountered by the probe pulse ($\delta n/n_0$, where n_0 is the ambient density) was up to 10^{-1}. This

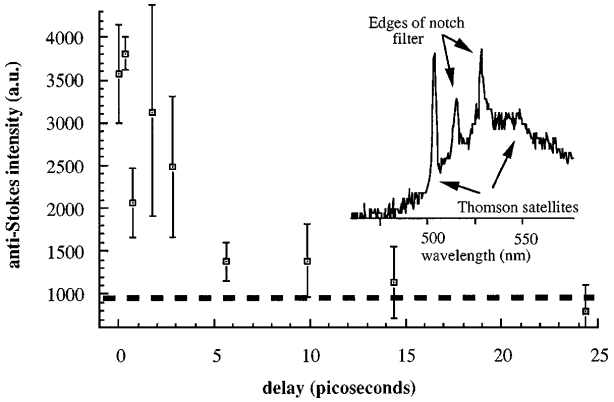

FIG. 2. Evolution of electron satellites from zero-degree Thomson scattering. The background level is shown by the dashed line. Data are not shown for pump-probe delay times less than zero since blueshifting of the probe laser spectrum saturates the detector for early times. Inset is a typical spectrum (anti-Stokes at 506 nm, Stokes at 550 nm).

is probably an underestimate of the actual amplitude of the wakefields produced in these experiments since slight misalignments in our setup can result in a substantial reduction of signal.

In the second CTS configuration, the scattered light was observed at a convenient forward scattering angle of 30° ± 5° from the pump-probe axis by relocating the collection optics shown in Fig. 1. The wakefields generated in these experiments are highly three dimensional due to the tight focusing of the pump laser. This causes a strong radial profile of the wakefield which implies that the scattering plasma waves have significant $\mathbf{k}_\perp$ components ($\sim 2\pi/r_0$, r_0 being the pump laser focal spot radius) and lower phase velocities. At 30°, the phase velocity can vary from $0.06c$ to $0.49c$ from consideration of the f numbers of the alignment and detection optics. These lower phase velocity plasma waves couple more readily with the probe laser to scatter in the near forward directions. In fact, a 10° tilt between the pump and probe lasers by displacing the probe laser on the focusing parabolic mirror (while maintaining the 30° angle to the pump for the scattered light) gave a better signal to noise ratio without changes to the general behavior of the scattered signal.

As shown in the inset in Fig. 3, when the probe laser was injected at delay = +1 ps, there is a marked increase in the emission of the first order electron satellites. Electron satellite emission lasted for about 5–7 ps in both hydrogen and helium, similar to that observed in the directly forward direction, as shown by the closed circles in Fig. 3. A low level of satellite emission was also observed to be generated by the pump laser alone from its interaction with plasma density gradients due to filamentation and charge displacement effects [16].

The inset in Fig. 3 also shows a dramatic rise in the central peak of the Thomson scattered spectrum which correlates to the decline of the electron plasma sidebands. We believe this central peak is due to coherent Thomson scattering from ion acoustic waves since both a strong dependence on the polarization of the probe beam and a dependence of its intensity on n_e^2 were observed. The open circles in Fig. 3 show that the amplitude of the central scattered peak reached a maximum at $\Delta t \approx 25$ ps after the main pulse for hydrogen and at $\Delta t \approx 40$ ps for helium. We believe this is due to the turbulent decay of the forward going large amplitude plasma waves into ion acoustic waves through mechanisms such as the modulational instability.

Significant theoretical work has been performed on the decay of large amplitude Langmuir waves via parametric coupling to ion acoustic waves [17,18]. In particular, for moderate temperatures ($T_e < 1$ keV), a Langmuir wave is subject to the modulation instability (MI) [17], in which a plasma wave $(\omega_p, \mathbf{k}_p)$ decays into a low-frequency ion wave $(\omega_i, \mathbf{k}_i)$ and two daughter electron plasma waves $(\omega_p \pm \omega_i, \mathbf{k}_p \pm \mathbf{k}_i)$, where typically $k_i \gg k_p$. Ion waves generated by MI have been observed coincident with plasma waves in experiments on the plasma beat-

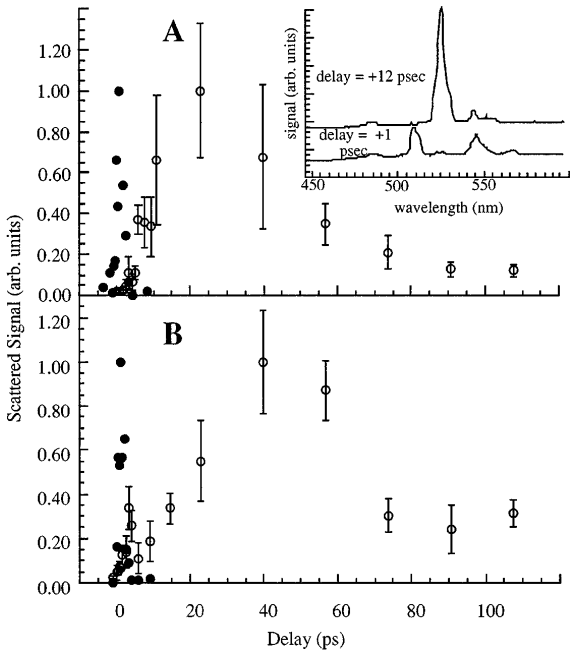

FIG. 3. Evolution of Thomson scattered spectrum at 30° angle with respect to pump laser: (a) hydrogen; (b) helium. Open circles are normalized values of the central peak in the scattered spectrum and closed circles are the normalized value of the first order Stokes satellite. Inset shows examples of typical Thomas scattered spectra for the delay times indicated.

wave accelerator [11]. In these experiments, the plasma wave is simultaneously driven by the long duration laser pulses (~150 ps) while decaying via MI. In SM-LWFA experiments, on the other hand, the plasma waves are first generated very rapidly (<1 ps) and then decay into ion waves in the region behind the laser pulse. Collisional damping of the wakefield can be neglected since, for electrons oscillating in a $\delta n/n_0 \sim 0.1$ plasma wave, the electron-ion collision time is long (typical ~300 ps).

The linear growth rate [18] of MI depends on the parameter $v_L/v_{te} = 23(\delta n/n_0)T_e^{-1/2}$, where T_e is the electron temperature in keV, v_L is the electron quiver velocity in the Langmuir wave, and v_{te} is the electron thermal velocity. MI occurs in the strong field limit when $v_L/v_{te} > (\omega_{pe}/\omega_{pi})^{1/3}$, where ω_{pe} and ω_{pi} are the plasma frequencies for the electrons and ions, respectively. Initially, if the plasma wave amplitude is large ($\delta n/n_0 \sim 0.1$) and for $T_e \sim 10$ eV, the strong field condition is satisfied such that $v_L/v_{te} \sim 23$ and $(\omega_{pe}/\omega_{pi})^{1/3} \sim 3$. The maximum strong field growth rate [18] is given approximately by the ion plasma period ($\gamma_{sf} \sim \omega_{pi}$) and the corresponding e-folding time $\tau_{sf} = 1/\gamma_{sf}$ is short, about 0.3 ps for H_2 ($2\pi/\omega_{pi} = 1.8$ ps) and about 0.4 ps for He ($2\pi/\omega_{pi} = 2.5$ ps).

As the initial wakefield decays, however, $\delta n/n_0$ decreases and MI transitions [18] to the slower growth of the weak field limit, $v_L/v_{te} < (\omega_{pe}/\omega_{pi})^{1/3}$, with a maximum weak field growth rate of $\gamma_{wf} \sim 6^{-1/2}\omega_{pi}(v_L/v_{te})$. Notice that as $\delta n/n_0$ ($\sim v_L/v_{te}$) decreases, so does the

growth rate. In addition, the decay of the wakefield behind the laser pulse is likely to be accompanied by electron plasma heating, which will also decrease the growth of MI. The daughter plasma waves may also decay and hence can lead to a cascade of the wakefield energy into smaller amplitude daughter waves and drive ion waves over longer time scales. For example, $\delta n/n_0 \sim 10^{-3}$ and $T_e = 100$ eV give $\tau_{\rm wf} = 1/\gamma_{\rm wf} \sim 8$ ps for H_2 (11 ps for He) which agree reasonably well with the time scales shown in Figs. 3(a) and 3(b).

The temporal behavior of the central scattered peak shown in Fig. 3 may also be affected by the formation of a plasma channel. Detailed measurements of plasma channel formation in these experiments are discussed elsewhere [19]. As a brief account, Thomson scattered emission from the *pump* laser was imaged onto the 90° CCD camera shown in Fig. 1. An extended propagation channel of about 2.5 mm (about the width of the gas jet) was observed as the pump laser power was increased to ~2 TW. When the probe was injected along with the pump ($P_{\rm probe} \ll P_c$), Thomson scattered emission from the *probe* pulse at 527 nm was observed throughout the region where channeling of the high intensity pump pulse occurred. Its intensity increased to a maximum for probe delays of ~15 ps and subsequently decayed over about 50 ps [19]. This long lived waveguide structure [20] is probably formed by the following mechanism. As the pump pulse propagates, its ponderomotive force radially expels electrons. This creates a strong space charge field which initiates an outward radial motion of the ions. After the passage of the pump pulse, the ions continue to drift radially. Estimates indicate that the maximum depth of the plasma channel Δn is large, $\Delta n/n_0 > 0.5$, as is necessary to guide a tightly focused ($r_0 \sim 5\ \mu$m) probe laser pulse. The time scale for the formation of a plasma channel can be shown [19] to be for He ~26 ps (18 ps for hydrogen). Since the plasma channel guides the probe laser pulse for longer propagation distances L_z and $I_s \sim L_z^2$, the CTS signal will be enhanced as the channel is being formed, as is shown in Fig. 3.

In conclusion, these experiments have resulted in the first direct measurement of plasma waves generated by a LWFA in the self-modulated regime ($n_0 \sim 10^{19}$ cm^{-3}) using coherent Thomson scattering of a short (<1 ps) frequency-doubled probe laser pulse. By delaying the probe pulse with respect to the pump pulse, the time evolution of the plasma wave was measured. The lifetime of the wakefield was observed to be about 5 ps. The generation of ion waves was also measured over longer time scales, and is consistent with the theory of parametric decay of electron plasma waves via the modulation instability and the enhancement of the signal due to possible plasma channel formation.

The authors would like to thank J. Grun, A. Fisher, C. Manka, and H. Milchberg for useful discussions, and L. Daniels, K. Evans, and M. Baine for technical assistance. This work was supported by the Office of Naval Research and the U.S. Department of Energy.

[1] *Advanced Accelerator Concepts,* edited by P. Schoessow, AIP Conf. Proc. No. 335 (AIP, New York, 1995).
[2] T. Tajima and J. M. Dawson, Phys. Rev. Lett. **43**, 267 (1979); P. Sprangle, E. Esarey, A. Ting, and G. Joyce, Appl. Phys. Lett. **53**, 2146 (1988).
[3] P. Sprangle, E. Esarey, J. Krall, and G. Joyce, Phys. Rev. Lett. **69**, 2200 (1992); T. M. Antonsen and P. Mora, Phys. Rev. Lett. **69**, 2204 (1992); N. E. Andreev *et al.,* JETP Lett. **55**, 571 (1992); W. B. Mori *et al.,* Phys. Rev. Lett. **72**, 1482 (1994); E. Esarey, J. Krall, and P. Sprangle, Phys. Rev. Lett. **72**, 2887 (1994).
[4] J. Krall, A. Ting, E. Esarey, and P. Sprangle, Phys. Rev. E **48**, 2157 (1993).
[5] C. A. Coverdale *et al.,* Phys. Rev. Lett. **74**, 4659 (1995); A. Modena *et al.,* Nature (London) **377**, 606 (1995).
[6] K. Nakajima *et al.,* Phys. Rev. Lett. **74**, 4428 (1995).
[7] J. R. Marques *et al.,* Phys. Rev. Lett. **76**, 3566 (1996); C. W. Siders *et al.,* Phys. Rev. Lett. **76**, 3570 (1996).
[8] P. Maine *et al.,* IEEE J. Quantum Electron. **QE-24**, 398 (1988).
[9] C. E. Clayton *et al.,* Phys. Rev. Lett. **54**, 2343 (1985); M. Everett *et al.,* Nature (London) **368**, 527 (1994).
[10] F. Amiranoff *et al.,* Phys. Rev. Lett. **68**, 3710 (1992); F. Moulin *et al.,* Phys. Plasma **1**, 1318 (1994).
[11] J. Sheffield, *Plasma Scattering of Electromagnetic Radiation* (Academic Press, New York, 1975).
[12] W. Wood, C. Siders, and M. Downer, Phys. Rev. Lett. **67**, 3523 (1991); E. Esarey, G. Joyce, and P. Sprangle, Phys. Rev. A **44**, 3908 (1991).
[13] D. M. Villeneuve, H. A. Baldis, J. E. Bernard, and R. Benesch, J. Opt. Soc. Am. B **8**, 895 (1991).
[14] F. Martin, T. W. Johnston, and E. Ebrahim, Phys. Rev. Lett. **55**, 1651 (1985); C. E. Clayton, C. Joshi, C. Darrow, and D. Umstadter, Phys. Rev. Lett. **55**, 1652 (1985).
[15] R. E. Slusher and C. M. Surko, Phys. Fluids **23**, 472 (1980).
[16] J. Meyer and Y. Zhu, Phys. Fluids **30**, 890 (1987); K. Krushelnick, A. Ting, H. R. Burris, A. Fischer, C. Manka, and E. Esarey, Phys. Rev. Lett. **75**, 3681 (1995).
[17] V. D. Shapiro and V. I. Shevchenkoin *Handbook of Plasma Physics,* edited by A. A. Galeev and R. N. Sudan (North-Holland, New York, 1984), Vol. II; V. E. Zakharov, Zh. Eksp. Teor. Fiz. **62**, 1745 (1972) [Sov. Phys. JETP **35**, 908 (1972)].
[18] P. Mora *et al.,* Phys. Rev. Lett. **61**, 1611 (1988); D. Pesme *et al.,* Lasers Part. Beams **6**, 199 (1988).
[19] K. Krushelnick, A. Ting, C. I. Moore, H. R. Burris, E. Esarey, P. Sprangle, and M. Baine, Naval Research Laboratory Report No. (NRL/MR/96-7879) (to be published).
[20] C. G. Durfee III and H. M. Milchberg, Phys. Rev. Lett. **71**, 2409 (1993).